表 6　眼内レンズの選択

| 年齢，水晶体 | 嚢内固定 | 嚢外固定 | IOL 度数 | 術後矯正 |
|---|---|---|---|---|
| 1 歳未満，水晶体形成不全 | SA30AT | 3 ピースアクリル | ほぼ全例＋ 28D | 眼鏡（2 歳未満眼前 1 m，2 歳以降二重焦点） |
| 1 歳以上 | 1 または 3 ピースアクリル | | 術後正視狙い（ただし＋ 28D を最大度数とし，28.5D 以上は挿入しない | |

ない。あくまでも術後矯正として眼鏡を使用することを前提としている。

術後屈折矯正：眼軸長と水晶体の度数は，生直後が 17 mm 前後，＋35～40D で，その後 2 歳でも 20～21 mm，＋26～28D であり，2 歳以下では最大度数＋28D の IOL を挿入しても度数不足で術後に遠視となる場合が多い。また先天白内障症例は，術前から強い角膜直乱視を有している症例が多い。術後に残った遠視や乱視は，私の場合，ほとんどすべて眼鏡で矯正している。早期手術例では，遠視が＋10D 前後も残ってしまうため，片眼性症例では術後に大きな左右差を生じてしまう。この場合は，コンタクトレンズによる矯正も考慮する。しかし 1 歳未満の術後の屈折度数変化は急速で，コンタクトレンズでの対処が難しい場合も少なくない。また片眼性症例では術後に良好な両眼視機能を得ることは非常に困難で，両眼視機能はほとんど望めないのが現状であり，視力発達のみを目指すのであれば，左右差の強い眼鏡でも問題がない。さらに，コンタクトレンズは，脱着操作，管理が難しくコストも高い。そのため最近では全症例で眼鏡を使用している。術後の屈折変化に対応して眼鏡を作りかえる必要があるが，2 歳までは変化が急激なので何回か眼鏡を処方し直す必要があり，コストが安い単焦点の眼鏡を焦点距離が眼前 1 m となるように処方する。2 歳以降は屈折変化が緩徐となり比較的安定するので，遠近両用の 2 重焦点眼鏡を処方するのが最も適切な屈折矯正であると考えている（表 6）。

日本白内障学会誌 23：33～39，2011

# 調節性眼内レンズ

*Accommodating Intraocular Lens*

永本敏之*

## はじめに

現在の白内障手術は，手術機械，手術法と眼内レンズの進歩に伴って術後状態は飛躍的に改善した．現在の眼内レンズを人工水晶体と表現する眼科医もいる．人工レンズであることは間違いないが，人工水晶体とは言い難い．その理由は，本来水晶体は屈折機能，紫外線吸収機能，隔壁機能（房水と硝子体を分離する生理的隔壁）のほかに調節作用を有している．しかし現在市販されている眼内レンズは前3者の機能は兼ね備えているが，最後の調節機能を欠いているため人工水晶体とよぶには相応しくないと考えられるからである．調節機能の代用として遠近2焦点を有する多焦点眼内レンズが臨床応用されているが，あくまでも2焦点であり，調節機能には遠く及ばない．そのため調節機能を持った夢の眼内レンズ，まさしく人工水晶体とよぶのに相応しいレンズ（調節性眼内レンズ）の開発も盛んに行われている．

ここでは現在開発されている調節性眼内レンズのいくつかをご紹介したい．

## I 調節原理

調節作用を有する眼を持つ動物はほとんどなく，サルやヒトだけである．ヒトの調節作用の原理として最有力視されているのは，Helmholtzの原理であり，その主たる原理は，近見時に毛様体輪状筋の収縮に伴ってZinn小帯が弛緩し，水晶体は独自の弾性に従って厚さが増大するとともに表面曲率が増加して，屈折力も増加するというものである．従たる原理は，毛様体縦走筋の収縮に伴って毛様体の前方移動が起き，それに伴って水晶体も前方移動することによって近方に焦点がずれるという機能である．

調節性眼内レンズの作用原理も毛様体・Zinn小帯の動きを利用して焦点距離を変えようとするものがほとんどであるが，大きく分けると「表面曲率の増大」に伴う調節作用を起こそうとするレンズ（表面曲率増大型）と，「前方移動」に伴う調節作用を起こそうとするレンズ（前方移動型）に大別される．

## II 表面曲率増大型調節性眼内レンズ

このタイプのレンズは非常に古くから研究されており，日本人も多く関わっている．代表的なタイプは水晶体嚢内充填型である．これは，水晶体前嚢を小さく切除し，水晶体内容を除去してから，中にシリコーンなどでできた薄いバルーンを挿入してその中に，あるいはバルーンを挿入せずに直接水晶体嚢内に，液状またはゲル状の透明なポリマーを充填するというタイプで，古くは1964年のKesslerの報告[1,2]に始まり，日本でも西[3-11]，原[12]，属[13]らの報告がある（図1）．このタイプのレンズの課題は，①注入量およびバルーンの大きさ（個体差にどのように対応するのか），②光学精度（いかにしてきれいな結像を全調節域において得るのか），③術後正視にする方法（毛様体筋弛緩時には正視になっているのが理想的であるが，もし単純に術後も元の水晶体の屈折度になるのであれば，術前近視の人は術後も近視，術前遠視の人は術後も遠視になってしまう），④十分な調節力が得

*Toshiyuki Nagamoto：杏林大学医学部眼科学教室
〔別刷請求先〕永本敏之：〒181-8611 三鷹市新川6-20-2 杏林大学医学部眼科学教室

図1　シリコーンバルーン

られるか，⑤後発白内障の発生を予防できるか，⑥眼内における安全性，⑦簡単・確実な手術方法の確立，など多くの課題を残しており，臨床試験までにはまだまだ遠いというのが現状である．

次は最近開発されたNuLens[TM]である[17]．このレンズは，図2bに示したような複雑な形状をしている．オリジナルのレンズは支持部と光学部の前後面がハードな素材（PMMA）でできており，前後面に挟まれた光学部の中央にはソフトなシリコーンゲルが充填されている．PMMA光学部前面中央に円形の小さな窓が開いており，シリコーンが顔を出している．支持部は毛様溝に固定され，前後嚢の上に光学部が位置するという設計である．毛様体筋が弛緩すると残存水晶体嚢が緊張し，PMMA光学部後面を圧迫する．図2aに示したように光学部後面が圧迫されると前面に開いた小さな円形窓の部分からソフトなシリコーンゲルが球状に突出し，この部分の屈折度が増大するというのが，このレンズの原理である．非常に小さな範囲が突出するので度数変化は大きく，図2cに示したサルの実験では最大約40Dの屈折変化が得られるとしている[18]．またヒト眼での臨床治験（10眼）でも平均約10Dの調節力が得られたと報告されている[19]．しかし問題点も多い．まず第1に通常の調節とは逆で，毛様体筋が弛緩したときに屈折力が増大し，近方に焦点が移動することが欠点である．第2の欠点としては，後発白内障の発生率の高さである．10眼中6眼は1年以内にYAGレーザーによる後嚢切開が必要になったと報告されている[19]．たとえYAGレーザーが必要な後発白内障が起きなかったとしても術後の水晶体嚢は線維化が起き，硬くなるのが通常である．水晶体嚢が硬くなって

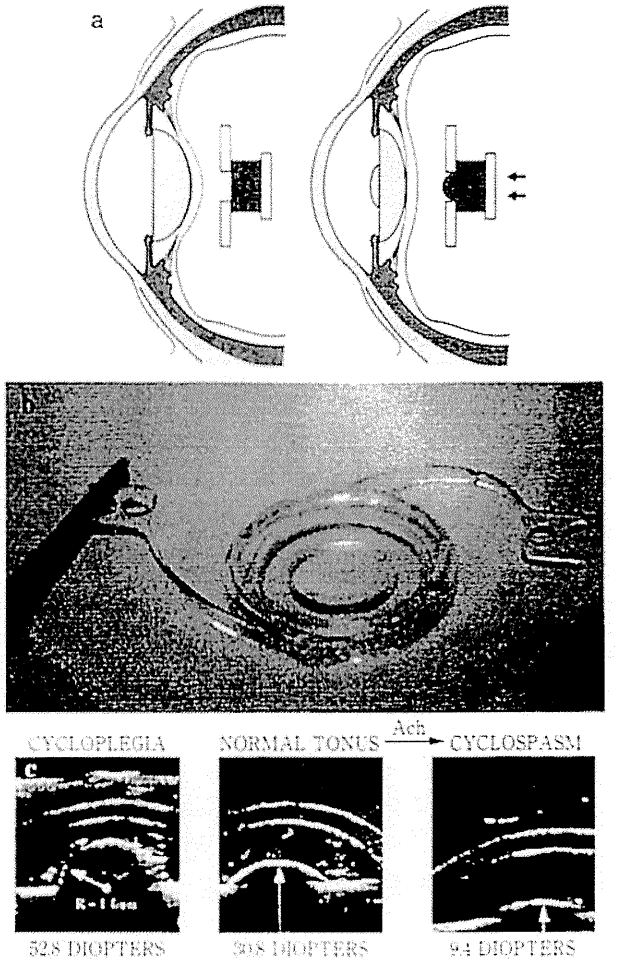


図2　NuLens[TM]

a：作用原理．光学部後方が圧迫されると光学部前方中央が突出する．b：全体像．c：光学部中央のカプセルの突出を示す前眼部OCT．左図は調節麻痺剤点眼時，右図は縮瞳剤（調節誘発剤）点眼時．

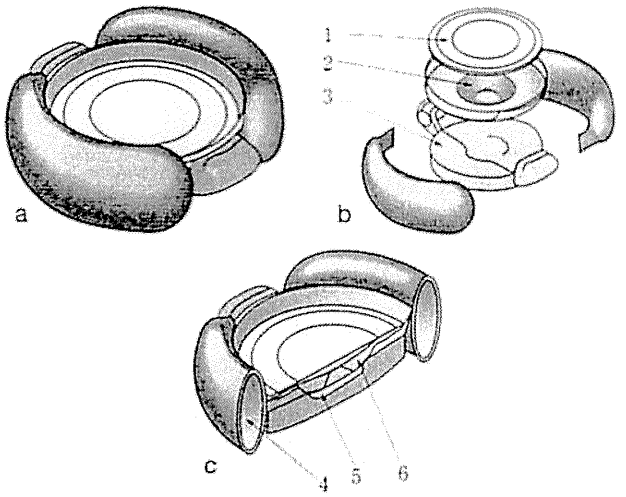


図3　FluidVision lens
a：全体像．b：構成．光学部は3つのパーツ（1～3）より成る．c：支持部内部（4），光学部間（5, 6）は液体が入っており，繋がっている．

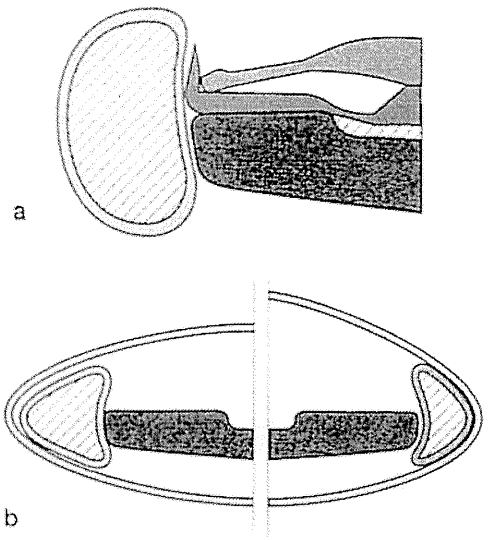


図4　FluidVision lensの作用原理
a：支持部内の空間と一番後方の光学部上の空間は繋がっている（斜線部分）．b：左図は遠見視，右図は近見視．近見時に水晶体嚢からの圧迫で支持部内の液体が少なくなる．減った分の液体は一番後方の光学部上の空間へと流れる．

しまうと毛様体筋の緊張と弛緩による水晶体嚢の変化は小さくなることが予想される．このことは，徐々に調節力が小さくなることを意味する．またYAGで後嚢を切開してしまえば，必然的に調節力は減少する．第3の欠点は切開創の大きさである．支持部と光学部外縁がハードなオリジナルレンズを挿入するためには9mmの切開が必要である．現在ソフトタイプが開発され，4mmの切開から挿入が可能になったと言われているが，それでも小切開とは言い難い．第4の欠点は，有効光学面積の小ささである．以上のようにこのレンズにはまだ欠点が多く，一般化するには問題が多すぎる．

次はさらに新しいFluidVision™ lensである．このレンズはNuLens™とは違って，水晶体嚢内に挿入するタイプのレンズであり，ヒト眼と同様に毛様体筋の収縮時に調節作用が起きる．しかし，光学部の中央部分が突出することによって調節作用を得るという点ではNuLens™と同様である．このレンズは図3aに示したように非常に複雑な形状をしている．図3bに示したように光学部は3つのパーツで構成されている．その周りを囲むように支持部が配置されている．図3cに示したように3つの光学部の間には空洞があり，この中は液体で満たされている．また支持部は袋状の構造で，この中も液体で満たされており，一番後方の光学部と中間の光学部の間の空間と繋がっている（図4a）．図4bに示したように毛様体筋の緊張に伴ってZinn小帯が弛緩すると水晶体嚢は厚さが増大する方向に形状変化を起こすが，その際に支持部の内容積が減少し，光学部間に液体が流入し，比較的厚くて硬い一番後方の光学部は変化せずに薄くて柔らかい中間の光学部の中央が前方に押し上げられ，さらには一番前方の光学部の中央も突出するために屈折度が増大し，調節が得られるというのがこのレンズの原理である．臨床治験で5眼に挿入し，術後1カ月で全例5～8Dの調節があったと報告されているが，インターネット上での情報であり詳細は不明である（http://voi.opt.uh.edu/14_Scholl_FluidLens/14_SchollFluidLensConcept.pdf#search='FluidVision lens'）．

## III　前方移動型調節性眼内レンズ

このタイプには通常の眼内レンズと同様に1枚の光学部のタイプ（1枚型）と2枚の光学部を持つタイプ（2枚型）に大別される．

### 1．1枚型前方移動型調節性眼内レンズ

1枚型はすでに欧米では発売され臨床応用されている

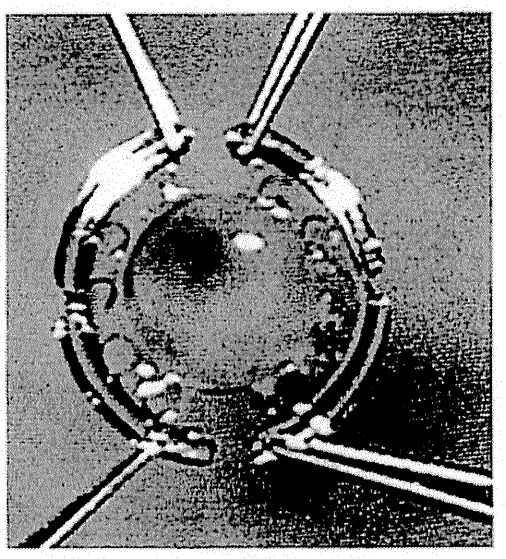

図5　BioComFold[8]（1996，Morcher社）

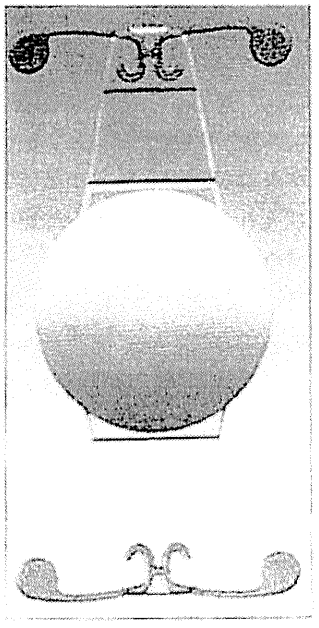

図7　AT-45 CrystaLens[9]（2002，Eyeonics社，その後B&L社）

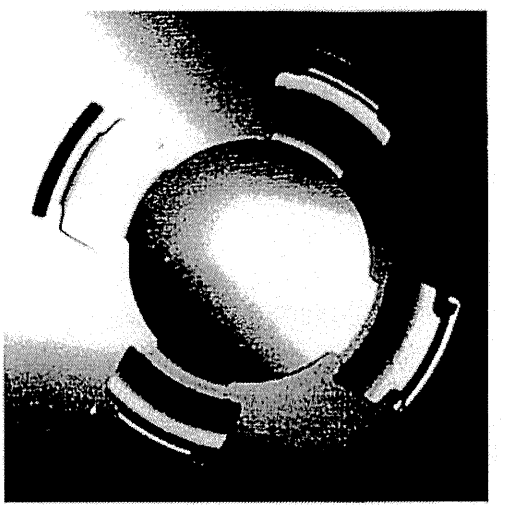

図6　ICU[7]（2001，HumanOptics社）

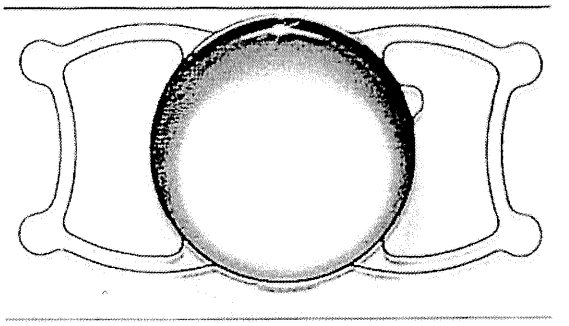

図8　Tetraflex[2]（Lenstec社）

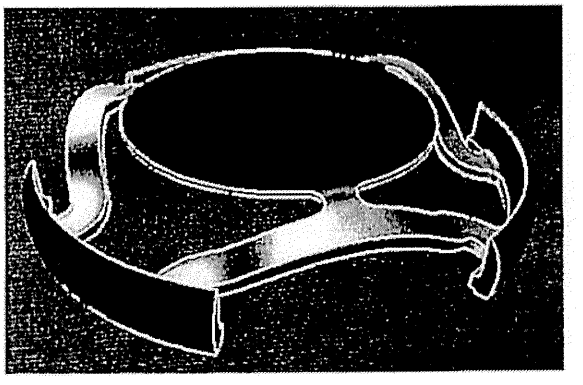

図9　OPAL-A[8]（Bausch & Lomb社）

が，その成績は決して良いとは言えない．最初にBioComFold[8]（1996，Morcher社）（図5），その後ICU[7]（2001，HumanOptics社）（図6），AT-45 CrystaLens[9]（2002，Eyeonics社，その後B&L社）（図7）が発売され，Tetraflex[2]（Lenstec社）（図8），OPAL-A[8]（Bausch & Lomb社）（図9）も臨床治験の段階である．これらのレンズのデザインに共通しているのは，光学部と支持部の境にヒンジとなる部分を設け，毛様体筋の調節変化に応じて光学部の前方移動を起こそうとしていることである．臨床成績で共通しているのは，実質的なレンズの前方移動はほとんど起こっておらず，屈折度数の変化についてはほとんど報告がなく，客観的調節量は非常に少な

いが[20~24]，自覚的検査に基づく調節量は単焦点レンズと同等もしくはやや良好であるという点[20~32]と，後発白内障の発生率が非常に高いという点[25,26,28,31,32]である．何らかの理由により相当数の症例において比較的良好な近方視が得られており，患者の満足もある程度得られているようであるが，実質的な前方移動は得られず，調節を起こすために意図した機能は果たしてはいない．この点からするととても調節性眼内レンズとはよべず，後発白内障の高発生率の点からも良いレンズとは言えない．

### 2．2枚型前方移動型調節性眼内レンズ

2枚型レンズは，強いプラス度数（+32D）の前方レンズとマイナス度数を持った後方レンズから構成され，後方のマイナスレンズの度数を，患者の眼軸長と角膜曲率に応じて変化させることによって術後に正視を得る．前方レンズと後方レンズはブリッジングされており，毛様体筋の調節変化に応じて前方レンズが前方移動するように設計されている．代表的レンズは，Synchrony IOL[9]（Visiogen社，その後AMO社）（図10）とSarfarazi IOL[7]（Bausch & Lomb社）（図11）である．

1枚型と2枚型を比較した場合，2枚型には大きなメリットがある．1枚型レンズで術後に正視を得ようとすると，近視眼には弱い度数，遠視眼には強い度数のレンズが必要である．強い度数のレンズが1mm前方移動した場合と弱い度数のレンズが1mm前方移動した場合とでは，同じ1mmでも得られる屈折変化は大きく異なり，当然強い度数のレンズが1mm移動したほうが変化が大きくなる．たとえば+20Dのレンズが1mm前方移動しても1.4Dの調節しか得られないが，+32Dのレンズでは2.5Dの調節が得られる．このため+20Dのレンズで3Dの調節を得るためには2.2mmもの移動量が必要となる．1枚型に対して2枚型では，患者の状態とは関係なく前方レンズを一定の+32Dにしてあり，このレンズが移動した場合に大きな屈折変化が得られる（図12）．図中には前方レンズのみが移動する場合（実線）と前後両レンズが移動する場合（破線）が示されているが，ヒト眼の調節原理から推察すると主に前方レンズの前方移動のみが起こることが予想され，眼軸長に関係なくほぼ一定の調節量が得られることが予想される[33]．

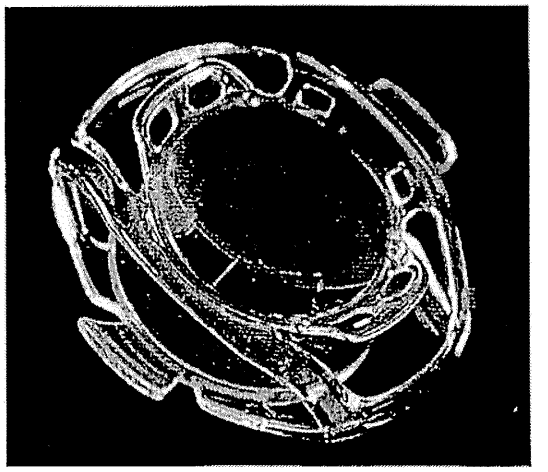

図10　Synchrony IOL[9]（Visiogen社，その後AMO社）

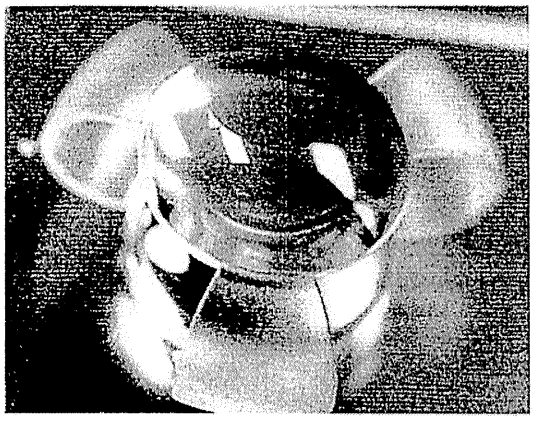

図11　Sarfarazi IOL[8]（Bausch & Lomb社）

しかし，水晶体嚢の大きさが異なると，水晶体嚢へのレンズのフィッティングが異なり，水晶体嚢の変化量とレンズの移動量の関係が変わることが予想される．たとえば，レンズに比べて水晶体嚢が大きすぎる場合は，水晶体嚢の変化はレンズにうまく伝わらず，調節量が少なくなると考えられる．したがって水晶体嚢の個体差への対応はかなり重要であると考えられる．

Synchrony IOL[9]を挿入した26眼で平均3.22D（1~5D）の自覚的調節力が得られたと報告されている[34]が，前方レンズの移動量や屈折値の変化は不明である．Sarfarazi IOL[7,35]についての臨床報告はまだない．

2枚型のレンズは理論的には1枚型よりも期待が持てるが，前方移動量が示されないと意図したように機能しているかどうかの判定はむずかしい．また，両レンズに

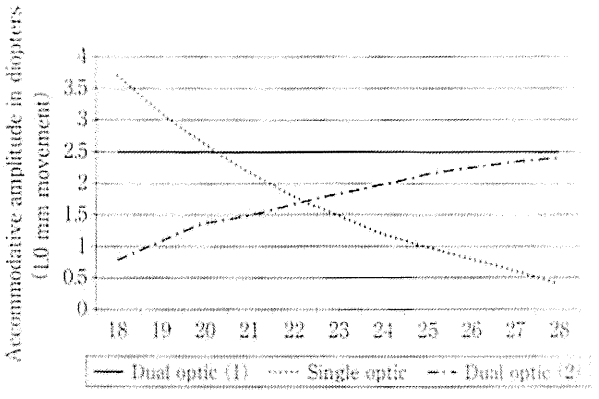


**図 12　1 枚型と 2 枚型前方移動型調節性眼内レンズの移動距離と屈折変化**

3 種類のレンズ（1 枚型と 2 枚型 2 種類）が 1.0mm 移動した場合の屈折量変化を示す理論的グラフ．横軸は眼軸長（mm）で，正視を得るための眼内レンズ度数を想定している．点線は 1 枚型の前方移動型レンズの場合で，強度近視になるにつれて正視を得るための度数が小さくなるため屈折量の変化も少なくなる．実線と破線は，2 枚型前方移動型レンズで前方レンズを＋32D に固定し，後方レンズのマイナス度数が眼軸長に応じて変化する場合を示している．実線は前方の＋32D レンズのみが 1.0mm 前方移動した場合の屈折量変化であり，眼軸長に関係なく約 2.5D の調節が得られる．一方，破線は前方レンズが 0.5mm 前方移動し，後方レンズも 0.5mm 後方移動した場合の屈折量変化を示している．後方のマイナスレンズが後方移動した場合も調節に寄与するが，短眼軸長眼ではマイナス度数が弱いため調節量が少なく，逆に長眼軸長眼では強いマイナス度数レンズを要するため，調節量も大きくなっている．

共通する欠点は，挿入のために大きな切開創を必要とする点である．Synchrony IOL[5] については後発白内障の発生率は非常に低いことが報告されている[35-37]が，Surfarazi IOL[3] については不明である．

## おわりに

まだ現段階では臨床的に満足できるような調節性眼内レンズはないが，近い将来登場する期待は十分にあると考えられ，今後の研究・開発の発展に期待したい．

## 文　献


1) Kessler J : Experiments in refilling the lens. *Arch Ophthalmol* **71** : 412-417, 1964
2) Kessler J : Refilling the rabbit lens. Further experiments. *Arch Ophthalmol* **76** : 596-598, 1966
3) Kessler J : Lens refilling and regrowth of lens substance in the rabbit eye. *Ann Ophthalmol* **7** : 1059-1062, 1975
4) Nishi O, Hara T, Hara T et al : Various kinds of experimental refilling lens with endocapsular balloon. *Dev Ophthalmol* **18** : 125-133, 1989
5) Nishi O : Refilling the lens of the rabbit eye after intercapsular cataract surgery using an endocapsular balloon and an anterior capsule suturing technique. *J Cataract Refract Surg* **15** : 450-454, 1989
6) Nishi O, Hara T, Hara T et al : Further development of experimental techniques for refilling the lens of animal eyes with a balloon. *J Cataract Refract Surg* **15** : 584-588, 1989
7) Nishi O, Hara T, Sakka Y et al : Refilling the lens with inflatable endocapsular balloon. *Dev Ophthalmol* **22** : 122-125, 1991
8) Nishi O, Hara T, Hara T et al : Refilling the lens with a inflatable endocapsular balloon : surgical procedure in animal eyes. *Graefes Arch Clin Exp Ophthalmol* **230** : 47-55, 1992
9) Nishi O, Nakai Y, Yamada Y et al : Amplitudes of accommodation of primate lenses refilled with two types of inflatable endocapsular balloons. *Arch Ophthalmol* **111** : 1677-1684, 1993
10) Nishi O, Nishi K, Mano C et al : Controlling the capsular shape in lens refilling. *Arch Ophthalmol* **115** : 507-510, 1997
11) Nishi O, Nakai Y, Mizumoto Y et al : Capsule opacification after refilling the capsule with an inflatable endocapsular balloon. *J Cataract Refract Surg* **23** : 1548-1555, 1997
12) Nishi O, Nishi K, Mano C et al : Lens refilling with injectable silicone in rabbit eyes. *J Cataract Refract Surg* **24** : 975-982, 1998
13) Nishi O, Nishi K : Accommodation amplitude after lens refilling with injectable silicone by sealing the capsule with a plug in primates. *Arch Ophthalmol* **116** : 1358-1361, 1998
14) Nishi O, Nishi K, Nishi Y et al : Capsular bag refilling using a new accommodating intraocular lens. *J Cataract Refract Surg* **34** : 302-309, 2008
15) Hara T, Sakka Y, Sakanishi K et al : Complications associated with endocapsular balloon implantation in rabbit eyes. *J Cataract Refract Surg* **20** : 507-512, 1994
16) Sakka Y, Hara T, Yamada Y et al : Accommodation in primate eyes after implantation of refilled endocapsular balloon. *Am J Ophthalmol* **121** : 210-212, 1996
17) Ben-Nun J : The NuLens accommodating intraocular lens. *Ophthalmol Clin North Am* **19** : 129-134, 2006
18) Ben-Nun J, Alió JL : Feasibility and development of a high-power real accommodating intraocular lens. *J Cataract Refract Surg* **31** : 1802-1808, 2005
19) Alió JL, Ben-nun J, Rodriguez-Prats JL et al : Visual and accommodative outcomes 1 year after implantation of an accommodating intraocular lens based on a new concept. *J Cataract Refract Surg* **35** : 1671-1678, 2009
20) Legeais JM, Werner L, Werner L et al : Pseudoaccommodation : BioComFold versus a foldable silicone intraocular

lens. *J Cataract Refract Surg* **25** : 262-267, 1999
21) Findl O, Kriechbaum K, Menapace R et al : Laserinterferometric assessment of pilocarpine-induced movement of an accommodating intraocular lens : a randomized trial. *Ophthalmology* **111** : 1515-1521, 2004
22) Kriechbaum K, Findl O, Koeppl C et al : Stimulus-driven versus pilocarpine-induced biometric changes in pseudophakic eyes. *Ophthalmology* **112** : 453-459, 2005
23) Sauder G, Degenring RF, Kamppeter B et al : Potential of the 1 CU accommodative intraocular lens. *Br J Ophthalmol* **89** : 1289-1292, 2005
24) Hancox J, Spalton D, Heatley C et al : Objective measurement of intraocular lens movement and dioptric change with a focus shift accommodating intraocular lens. *J Cataract Refract Surg* **32** : 1098-1103, 2006
25) Mastropasqua L, Toto L, Nubile M et al : Clinical study of the 1CU accommodating intraocular lens. *J Cataract Refract Surg* **29** : 1307-1312, 2003
26) Heatley CJ, Spalton DJ, Hancox J et al : Fellow eye comparison between the 1CU accommodative intraocular lens and the Acrysof MA30 monofocal intraocular lens. *Am J Ophthalmol* **140** : 207-213, 2005
27) Kamppeter BA, Sauder G, Jonas JB : Contrast and glare sensitivity after implantation of AcrySof and Human Optics 1CU intraocular lenses. *Eur J Ophthalmol* **15** : 458-461, 2005
28) Dogru M, Honda R, Omoto M et al : Early visual results with the 1CU accommodating intraocular lens. *J Cataract Refract Surg* **31** : 895-902, 2005
29) Wolffsohn JS, Naroo SA, Motwani NK et al : Subjective and objective performance of the Lenstec KH-3500 "accommodative" intraocular lens. *Br J Ophthalmol* **90** : 693-696, 2006
30) Marchini G, Mora P, Pedrotti E et al : Functional assessment of two different accommodative intraocular lenses compared with a monofocal intraocular lens. *Ophthalmology* **114** : 2038-2043, 2007
31) Hancox J, Spalton D, Heatley C et al : Fellow-eye comparison of posterior capsule opacification rates after implantation of 1CU accommodating and AcrySof MA30 monofocal intraocular lenses. *J Cataract Refract Surg* **33** : 413-417, 2007
32) Harman FE, Maling S, Kampougeris G et al : Comparing the 1CU accommodative, multifocal, and monofocal intraocular lenses : a randomized trial. *Ophthalmology* **115** : 993-1001, 2008
33) McLeod SD : Optical principles, biomechanics, and initial clinical performance of a dual-optic accommodating intraocular lens (an American Ophthalmological Society thesis). *Trans Am Ophthalmol Soc* **104** : 437-452, 2006
34) Ossma IL, Galvis A, Vargas LG et al : Synchrony dual-optic accommodating intraocular lens. Part 2 : pilot clinical evaluation. *J Cataract Refract Surg* **33** : 47-52, 2007
35) Sarfarazi FM : Sarfarazi dual optic accommodative intraocular lens. *Ophthalmol Clin North Am* **19** : 125-128, 2006
36) Werner L, Pandey SK, Izak AM et al : Capsular bag opacification after experimental implantation of a new accommodating intraocular lens in rabbit eyes. *J Cataract Refract Surg* **30** : 1114-1123, 2004
37) Bohórquez V, Alarcon R : Long-term reading performance in patients with bilateral dual-optic accommodating intraocular lenses. *J Cataract Refract Surg* **36** : 1880-1886, 2010

* * *

# Wound Architecture of Clear Corneal Incision With or Without Stromal Hydration Observed With 3-Dimensional Optical Coherence Tomography

SHINICHI FUKUDA, KEISUKE KAWANA, YOSHIAKI YASUNO, AND TETSURO OSHIKA

• PURPOSE: To evaluate wound architectures of a clear corneal incision and the duration of stromal edema caused by intentional hydration in cataract surgery using 3-dimensional (3-D) cornea and anterior segment optical coherence tomography (OCT).
• DESIGN: Prospective, randomized study.
• METHODS: On 30 eyes of 23 patients, cataract surgery was performed through a clear corneal incision created with a 2.4-mm blade. After confirming the water tightness of the clear corneal incision at the end of surgery, 15 randomly selected eyes received stromal hydration, and the remaining 15 eyes did not. Using the 3-D cornea and anterior segment optical coherence tomography, wound architecture was assessed 1 day, 1 week, and 2 weeks after surgery.
• RESULTS: There was a statistically significant difference in corneal thickness at the clear corneal incision between eyes with and without stromal hydration 1 day and 1 week after surgery ($P < .001$ and $P < .05$, Mann–Whitney $U$ test), but not at 2 weeks after surgery. On day 1, gaping at the epithelial side was seen in 6.7% (2 eyes), gaping at the endothelial side in 30% (9 eyes), misalignment of the roof and floor of incision in 40% (12 eyes), and local detachment of Descemet membrane in 36.7% (11 eyes). These imperfections improved with time.
• CONCLUSIONS: Using the 3-D cornea and anterior segment optical coherence tomography, detailed architectures of the clear corneal incision were investigated. It was found that the effect of stromal hydration lasted for at least 1 week after surgery. (Am J Ophthalmol 2011; 151:413–419. © 2011 by Elsevier Inc. All rights reserved.)

A SELF-SEALING CLEAR CORNEAL INCISION HAS BEEN used widely in cataract surgery because of ease of construction and lack of bleeding.[1] Surgeons typically check the wound integrity by inflating the anterior chamber with balanced salt solution and applying pressure with a Weck cell sponge (Eagle Laboratories, Rancho Cucamonga, California, USA) against the posterior lip of the incision. If apparent leakage exists, the surgeon often applies corneal stromal hydration to enhance wound sealing and to prevent the inflow of ocular surface fluid.[2–4] Proper construction and secure closure of the incision, including application of stromal hydration, are of critical importance to obtain optimal outcomes after cataract surgery. However, there have been only a few reports that investigated the detailed structure of the clear corneal incision using optical coherence tomography (OCT),[5–7] and it is not clear how long the effects of stromal hydration last.[8]

We developed a 3-dimensional (3-D) corneal and anterior segment OCT based on swept-source OCT technology, which is a variation of Fourier-domain OCT.[9,10] Because the measurement speed of swept-source 3-D corneal and anterior segment OCT is more than 10 times faster than that of time-domain OCT, it has high robustness against a sample motion and is capable of obtaining full 3-D images of ocular tissues.[9,11] The 3-D corneal and anterior segment OCT can create any cross-sectional images of the anterior segment of the eye, and thus it provides more precise perpendicular scans of the incision than the conventional imaging methods. In this study, 3-D corneal and anterior segment OCT was used to evaluate the detailed structural characteristics of clear corneal incision, including the duration of stromal hydration.

## METHODS

A TOTAL OF 30 EYES FROM 23 PATIENTS UNDERGOING standard cataract surgery were evaluated. The procedure was performed under topical anesthesia by a same surgeon (T.O.) at Tsukuba University Hospital. The research followed the tenets of the Declaration of Helsinki, and written informed consent was obtained from each eligible participant. The mean age of the participants was 71.1 ± 13.5 years of age (mean ± standard deviation). Inclusion criteria included no history of ocular surgery, maximum pupil dilation of more than 7.0 mm at the preoperative examination, absence of biomicroscopic signs of pseudo-

Accepted for publication Sep 13, 2010.
From the Department of Ophthalmology, Institute of Clinical Medicine, University of Tsukuba, Ibaraki, Japan (S.F., K.K., T.O.); the Computational Optics and Ophthalmology Group, Ibaraki, Japan (S.F., K.K., Y.Y., T.O.); and the Computational Optics Group, University of Tsukuba, Ibaraki, Japan (Y.Y.).
Inquiries to Shinichi Fukuda, Department of Ophthalmology, Institute of Clinical Medicine, University of Tsukuba, 1-1-1 Tennoudai, Tsukuba, Ibaraki 305-8575, Japan; e-mail: Caesar.ShihTzu@gmail.com

0002-9394/$36.00
doi:10.1016/j.ajo.2010.09.010

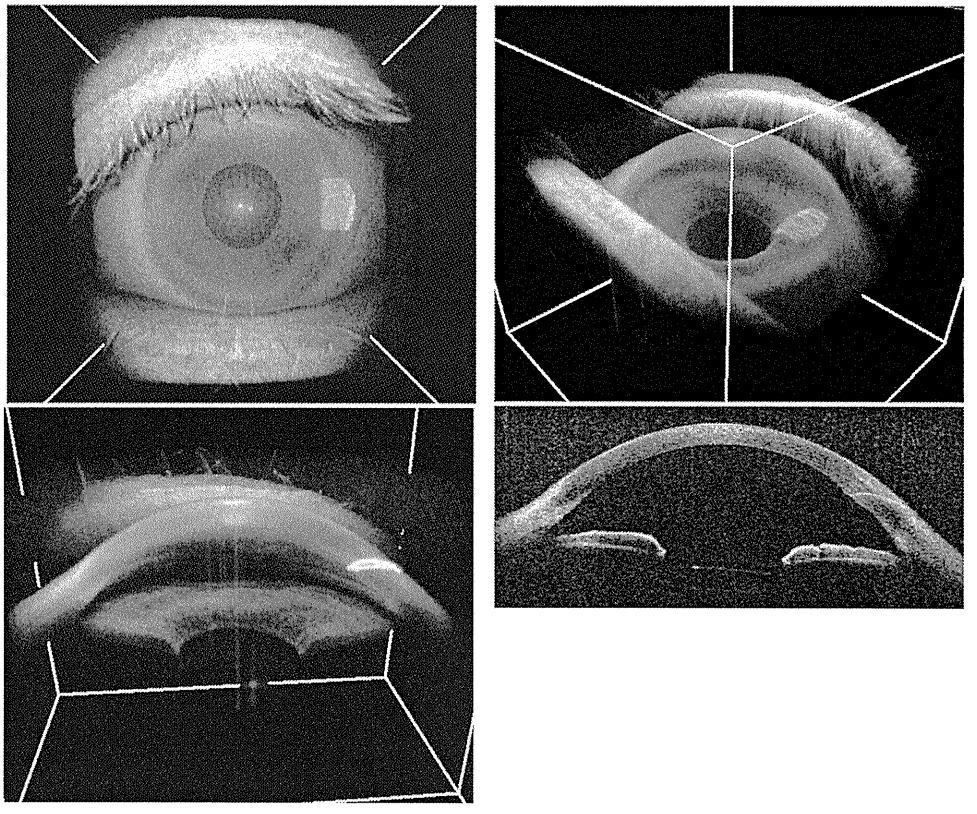

FIGURE 1. Images of clear corneal incision obtained by 3-dimensional cornea and anterior segment optical coherence tomography. (Top left, Top right, Bottom left) Three-dimensional images of anterior segment and clear corneal incision. (Bottom right) A 2-dimensional image can be obtained by sectioning the 3-dimensional image in any arbitrary direction.

exfoliation, normal fundus examination, and endothelial cell count of at least 2000 cells/mm$^2$. Exclusion criteria were the presence of preexisting corneal disease and of glaucoma.

Phacoemulsification and intraocular lens implantation were performed as follows. A side-port incision was created with a 30-degree steel blade. An ophthalmic viscosurgical device was injected into the anterior chamber, and then the main clear corneal incision with a square wound configuration was made using a 2.4-mm steel blade. Phacoemulsification was performed using OZil (Alcon, Fort Worth, Texas, USA) torsional technology with an ultrasleeve on an Infiniti phacoemulsification platform (Alcon). An intraocular lens (SN60WF; Alcon) was implanted using the D cartridge and Monarch injector. After the ophthalmic viscosurgical device was thoroughly washed out with an irrigation and aspiration unit, the anterior chamber was reformed with balanced salt solution through the paracentesis aiming for a slightly higher intraocular pressure. Intraocular pressure was checked digitally. At this stage, the wounds were checked for water tightness in all 30 eyes using a Weck cell sponge, and it was confirmed that all incisions had no leakage. Thereafter, corneal stromal hydration was applied in 15 randomly selected eyes by placing the tip of a 25-gauge cannula in the side walls of the incision and gently irrigating balanced salt solution into the stroma. This was performed at both edges of the incision. In the remaining 15 eyes, the wounds were not hydrated. The clear corneal incision was evaluated using the 3-D corneal and anterior segment OCT at 1 day, 1 week, and 2 week after surgery.

The 3-D corneal and anterior segment OCT was a custom prototype model built by the Computational Optics Group, University of Tsukuba,[9] and the Tomey Corporation (Nagoya, Japan), which was based on optical frequency-domain imaging technology.[10,12] The light source had a center wavelength of 1.3 μm, which enables greater penetration into the ocular tissue compared with the conventional 830 nm OCT. This system 3-dimensionally depicts the anatomic features of the anterior segment, such as cornea, scleral spur, angle recess, iris root, and filtering bleb.[13–15] The measurement speed is 20 000 A-lines/second. The maximum measurement ranges were 16 × 16 mm in width and 6 mm in depth in tissue. The mean axial resolution within a 4-mm depth range was 11 μm in tissue. The 3-D corneal and anterior segment OCT provided 3-D tomography with the acquisition time of 3.3 seconds per volume for 256 × 256 × 1024 voxels. A typical 3-D scan comprises 256 horizontal cross-sections, each of which comprises 256 A-scans. This OCT system can produce 2-dimensional images by sectioning the 3-D image in any arbitrary direction (Figure 1).

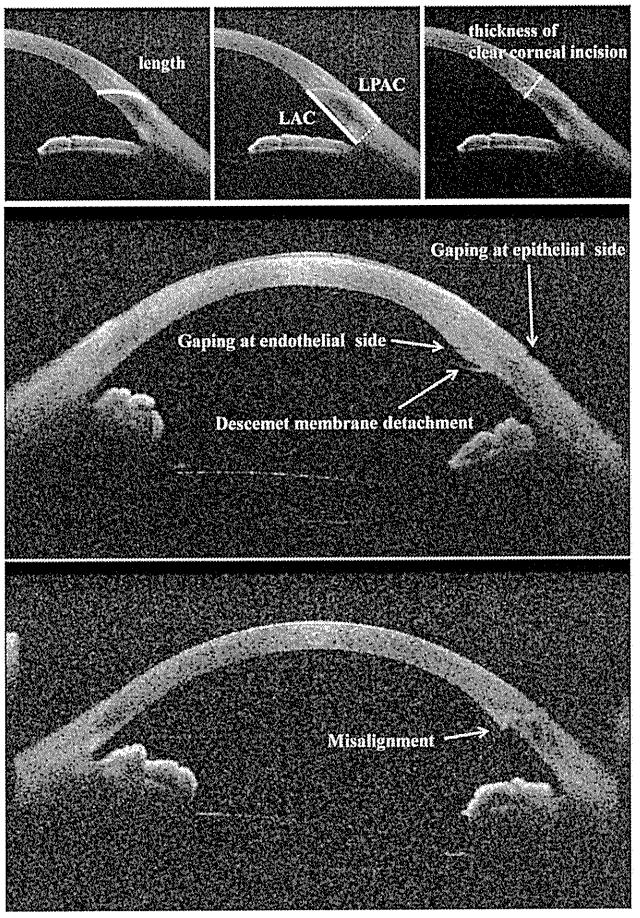


FIGURE 2. Two-dimensional images of clear corneal incision obtained by 3-dimensional cornea and anterior segment optical coherence tomography. (Top left) Length of clear corneal incision. Length between angle recess to endothelial side of clear corneal incision (LAC). (Top middle) Length between the point that drops a perpendicular line from angle recess to corneal surface and epithelial side of clear corneal incision (LPAC). (Top right) Corneal thickness at clear corneal incision. (Middle row) Gaping of the clear corneal incision at the epithelial side, gaping of the clear corneal incision at the endothelial side, and local detachment of Descemet membrane. (Bottom row) Misalignment of the roof and floor of the incision at the endothelial side.

The measurement parameters of the clear corneal incision included the length and width of the clear corneal incision, the length between angle recess to the endothelial side of the clear corneal incision, and the length between the point that drops a perpendicular line from the angle recess to the corneal surface and the epithelial side of the clear corneal incision (Figure 2).

Five architectural features of the clear corneal incision were assessed according to the report by Calladine and Packard: gaping of the wound at the epithelial and endothelial side, misalignment on the roof and the floor of the incision at the endothelial side, local detachment of the Descemet membrane, and loss of adaptation along the stromal tunnel (Figure 2).[16]

Table 1 summarizes preoperative characteristics of patients and surgery time. There were no significant differences in the baseline parameters between the stromal hydration group and the nonstromal hydration group. The measurement values of 2 groups were compared using the Mann–Whitney $U$ test. The 5 architectural features of the clear corneal incision were compared between 2 groups using the Fisher exact probability test. The intraocular pressure was compared in eyes with and without architectural features using the Mann–Whitney $U$ test. Analyses were carried out using StatView software (SAS Institute, Cary, North Carolina, USA).

## RESULTS

• CORNEAL THICKNESS AT CLEAR CORNEAL INCISION: In eyes with stromal hydration, corneal thickness at the clear corneal incision was 1020.5 ± 98.0 μm, 908.9 ± 54.4 μm, and 795.7 ± 57.6 μm at 1 day, 1 week, and 2 weeks after surgery, respectively. In eyes without stromal hydration, corneal thickness at the clear corneal incision was 880.3 ± 79.6 μm, 840.3 ± 92.0 μm, and 799.3 ± 93.6 μm at 1 day, 1 week, and 2 week after surgery, respectively. A statistically significant difference was noted between the 2 groups at 1 day and 1 week after surgery ($P < .001$ and $P < .05$, Mann–Whitney $U$ test; Figure 3). There was no significant difference between the 2 groups at 2 weeks after surgery ($P = 0.852$).

• WOUND ARCHITECTURE: Gaping at the epithelial and endothelial side was seen in 6.7% (2 eyes) and 30% (9 eyes) at 1 day after surgery (Figure 4). Misalignment of incision roof and floor at the endothelial side was seen in 40% (12 eyes), and local detachment of Descemet membrane was found in 36.7% (11 eyes). At 1 week after surgery, gaping at the epithelial side disappeared, and the percentage of eyes with gaping at the endothelial side and misalignment decreased to 13.3%. One patient showed local Descemet membrane detachment at 1 week and 2 week after surgery.

When eyes with (Figure 5) and without (Figure 6) stromal hydration were compared, eyes that received stromal hydration tended to show greater incidence, but there was no intergroup difference in the rate of gaping and misalignment ($P = .264$ at 1 day after surgery and $P = .598$ at 1 week after surgery, Fisher exact probability test), and local Descemet membrane detachment ($P > .999$ at all time points after surgery).

Table 2 summarizes the measurement results of clear corneal incision parameters. The length and width of the clear corneal incision were 2.56 ± 0.08 mm and 1.86 ± 0.18 mm, respectively. The length between angle recess to the endothelial side of the clear corneal incision and the length between the point that drops a perpendicular line

**TABLE 1.** Preoperative Characteristics of Patients, Surgery Time, and Intraocular Pressure in Eyes with and without Stromal Hydration

| | With Stromal Hydration | Without Stromal Hydration | All | *P* Value |
|---|---|---|---|---|
| Age (yrs) | 70.8 ± 12.3 | 71.4 ± 15.0 | 71.1 ± 13.5 | .740 |
| logMAR BCVA | 0.46 ± 0.23 | 0.42 ± 0.18 | 0.41 ± 0.23 | .659 |
| Surgery time (min) | 5.87 ± 1.30 | 5.93 ± 1.23 | 5.90 ± 1.24 | .848 |
| Preoperative IOP (mm Hg) | 12.6 ± 2.4 | 13.0 ± 2.3 | 12.8 ± 2.3 | .516 |
| Postoperative IOP (mm Hg) | | | | |
| 1 day after surgery | 17.9 ± 3.2 | 18.7 ± 2.1 | 18.3 ± 2.7 | .390 |
| 1 wk after surgery | 13.3 ± 2.5 | 13.1 ± 2.0 | 13.2 ± 2.2 | .866 |
| 2 wks after surgery | 12.4 ± 1.9 | 13.2 ± 1.6 | 12.8 ± 1.8 | .075 |
| Nuclear color | 2.43 ± 0.46 | 2.47 ± 0.69 | 2.45 ± 0.58 | .983 |
| Preoperative cell count (/mm$^2$) | 2701 ± 210 | 2815 ± 243 | 2758 ± 231 | .191 |

BCVA = best-corrected visual acuity; IOP = intraocular pressure; logMAR = logarithm of the minimal angle of resolution; wks = weeks; yrs = years.

Values are presented as mean ± standard deviation.

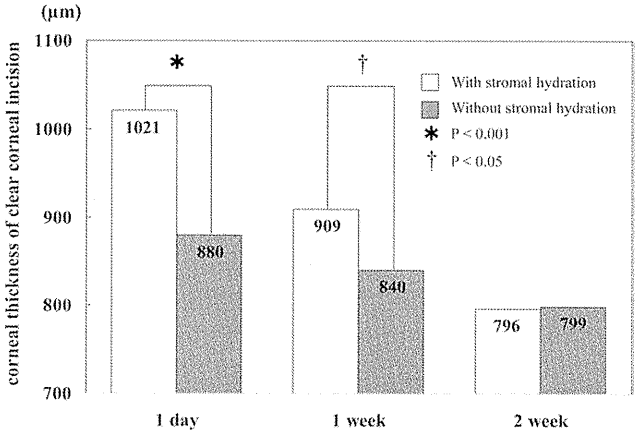


**FIGURE 3. Bar graph showing the time course of changes in corneal thickness at clear corneal incision using 3-dimensional cornea and anterior segment optical coherence tomography. A statistically significant difference was noted between eyes with and without stromal hydration at 1 day and 1 week after surgery ($P < .001$ and $P < .05$, Mann–Whitney $U$ test).**

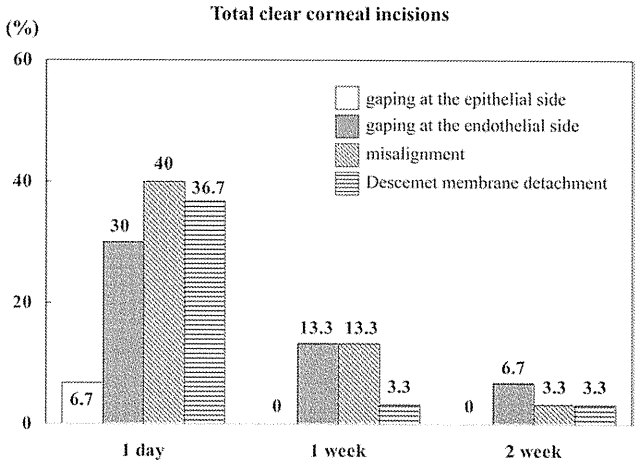


**FIGURE 4. Bar graph showing the time course of changes in the incidence of gaping, misalignment, and local detachment of Descemet membrane obtained by 3-dimensional cornea and anterior segment optical coherence tomography.**

from the angle recess to the corneal surface and epithelial side of the clear corneal incision were 2.63 ± 0.39 mm and 1.37 ± 0.27 mm, respectively. There were no significant differences in any parameters between eyes with and without stromal hydration.

Preoperative and postoperative intraocular pressure is summarized in Table 1. There were no significant differences in intraocular pressure between eyes with and without stromal hydration at any points ($P > .05$, Mann–Whitney $U$ test). Intraocular pressure at 1 day after surgery was 18.5 ± 0.7 mm Hg and 18.3 ± 2.8 mm Hg in eyes with and without gaping at the epithelial side, respectively. Intraocular pressure was 18.4 ± 2.1 mm Hg and 18.2 ± 3.0 mm Hg in eyes with and without gaping at the endothelial side, respectively. Intraocular pressure was 18.4 ± 3.1 mm Hg and 18.2 ± 2.5 mm Hg in eyes with and without misalignment, respectively. Intraocular pressure was 18.5 ± 2.5 mm Hg and 18.2 ± 2.9 mm Hg in eyes with and without local Descemet membrane detachment, respectively. These minor imperfections of the wound architecture did not influence intraocular pressure ($P > .05$, Mann–Whitney $U$ test).

## DISCUSSION

THERE HAD BEEN AN ANECDOTAL BELIEF THAT CORNEAL stromal hydration disappears within 1 to 2 hours after surgery. However, Fine and associates examined clear corneal incisions using Visante anterior segment OCT (Carl Zeiss Meditec, Dublin, California, USA) and dem-

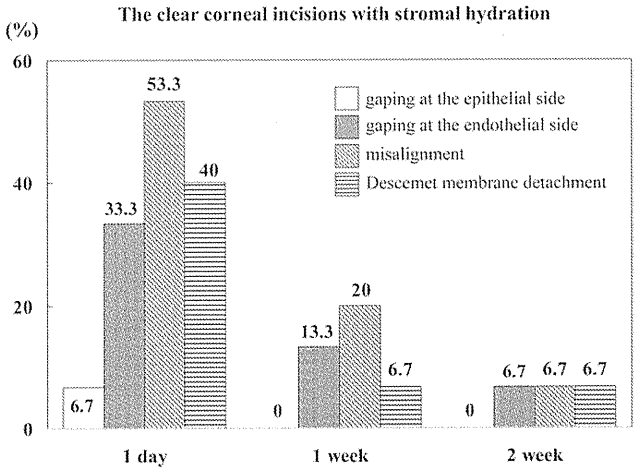


**FIGURE 5. Bar graph showing the time course of changes in the incidence of gaping, misalignment, and local detachment of Descemet membrane in eyes that received stromal hydration obtained by 3 -dimensional cornea and anterior segment optical coherence tomography.**

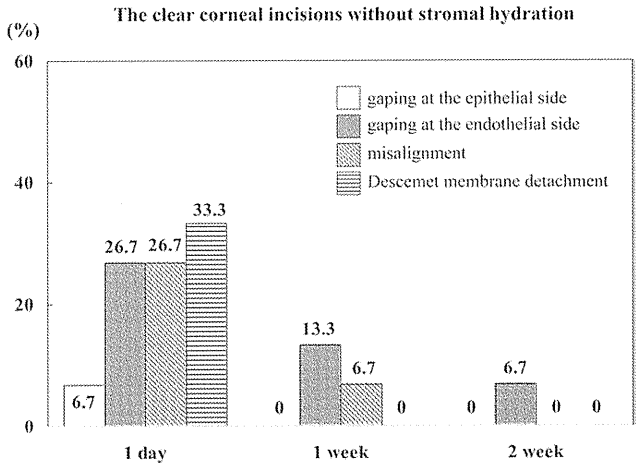


**FIGURE 6. Bar graph showing the time course of changes in the incidence of gaping, misalignment, and local detachment of Descemet membrane in eyes without stromal hydration obtained by 3-dimensional cornea and anterior segment optical coherence tomography.**

onstrated that stromal swelling lasted for at least 24 hours after surgery.[8] Because there has been no longitudinal study on the effect of corneal stromal hydration, it has not been clear how long stromal swelling continues after cataract surgery. In the current study, we investigated the architecture and pachymetry of clear corneal incisions using 3-D corneal and anterior segment OCT up to 2 weeks after surgery.

We found that corneal thickness at the clear corneal incision was increased significantly in eyes with stromal hydration compared with eyes without stromal hydration at 1 day and 1 week after surgery. At 2 week after surgery, there was no significant difference between the 2 groups. These results indicate that the effects of stromal hydration last for at least 1 week after surgery. The corneal thickness at the clear corneal incision in eyes with stromal hydration was 1020.5 ± 98.0 μm, 908.9 ± 54.4 μm, and 795.7 ± 57.6 μm at 1 day, 1 week, and 2 weeks after surgery, respectively. Dupont-Monod and associates measured corneal thickness at the wound level with Visante anterior segment OCT in eyes with stromal hydration after cataract surgery using 2.75-mm coaxial microincision, 2.20-mm coaxial microincision, and 1.30-mm bimanual phacoemulsification techniques.[17] At 1 day after surgery, the maximum corneal thickness at the clear corneal incision was 1074 ± 50 μm, 1012 ± 101 μm, and 1143 ± 140 μm, respectively. The pachymetry at 8 days after surgery recorded in 60% of patients was 908 μm, 865 μm, and 902 μm, respectively.[17] Their and our results are highly compatible in terms of changes in pachymetry at the wound level up to 1 week after surgery.

As shown in the Results, some imperfection of the wound architecture was found in the early postoperative period, such as gaping at the endothelial side, misalignment, and local Descemet membrane detachment. At 1 day after surgery, gaping at the endothelial side, misalignment, and Descemet membrane detachment were seen in 30% (9 eyes), 40% (12 eyes), and 36.7% (11 eyes) of the eyes, respectively, which decreased to 13.3% (4 eyes), 13.3% (4 eyes), and 3.3% (1 eye) at 1 week after surgery. Torres and associates reported that misalignment (imperfect apposition of the endothelial margin) was found in 45% of eyes on day 1 and in 15% of eyes on day 30,[7] which are in good agreement with our results. Misalignment was the result of a greater amount of stromal edema in the roof of the clear corneal incision than in the floor. In the current study, misalignment at the endothelial side was observed in 53.3% (8 eyes) in eyes with stromal hydration versus 26.7% (4 eyes) in eyes without stromal hydration. The incidence, however, was not significantly difference between the 2 groups. The incidence of other imperfections, such as gaping at the endothelial side and Descemet membrane detachment, did not differ between groups, either.

The gaping at the epithelial side was seen in only 6.7%, and disappeared 1 week later. A previous study demonstrated that epithelial gaping was found in 12%.[16] In their study, surgery was performed by 5 surgeons, 3 of whom were consultant grade and 2 of whom were juniors in training, whereas 1 experienced surgeon performed surgery in our study. We confirmed with 3-D corneal and anterior segment OCT that the incision angle, which was defined as the angle of the chord to a corneal tangent, was almost constant in the current series of patients, and the intraocular pressure was set slightly higher at the end of the operation. Previous in vivo and ex vivo studies using OCT imaging systems showed that improper incision angle or inappropriate intraocular pressure at the end of operation increased the risk of clear corneal incision gaping.[5–8]

**TABLE 2.** Dimension of Clear Corneal Incision Obtained by 3-Dimensional Cornea and Anterior Segment Optical Coherence Tomography

| | With Stromal Hydration | Without Stromal Hydration | All | *P* Value |
|---|---|---|---|---|
| Length (mm) | 1.82 ± 0.15 | 1.90 ± 0.19 | 1.86 ± 0.18 | .211 |
| Width (mm) | 2.59 ± 0.09 | 2.54 ± 0.06 | 2.56 ± 0.08 | .074 |
| LAC (mm) | 2.65 ± 0.43 | 2.61 ± 0.35 | 2.63 ± 0.39 | .934 |
| LPAC (mm) | 1.44 ± 0.24 | 1.30 ± 0.28 | 1.37 ± 0.27 | .097 |

LAC = length between angle recess to endothelial side of clear corneal incision; LPAC = length between the point that drops a perpendicular line from angle recess to corneal surface and epithelial side of clear corneal incision.

Local detachment of Descemet membrane was found in 36.7% (11 eyes) on day 1 and in 3.3% (1 eye) on days 7 and 14 after the surgery. Severe detachment of Descemet membrane is potentially a serious complication of intraocular surgery,[18] which is clinically considered to be rare in cataract extraction.[19–21] However, small incidental Descemet membrane detachment that could not be identified by biomicroscopy was found by gonioscopy in 47% of cases during routine cataract surgery.[22] In our study, the 3-D corneal and anterior segment OCT detected local Descemet membrane detachment in 40%. The high detection rate seems to be the result of its high resolution and ability to acquire images 3-dimensionally. Compared with contact gonioscopy, the 3-D corneal and anterior segment OCT is a noncontact and noninvasive method, reducing the risk of infection when examining clear corneal incision architecture immediately after surgery. Mackool and Holtz classified Descemet membrane detachment as planar when there is 1 mm or less separation of the Descemet membrane from its overlying stroma in all areas, whereas they defined it as nonplanar when Descemet membrane detachment exceeds 1 mm of separation.[23] They described planar detachments as having a much better prognosis than nonplanar detachments. In our cases, only small planar detachments were seen, which quickly and spontaneously reattached in almost every case. Dupont-Monod and associates reported that Descemet membrane detachment was seen in 51% of eyes at 1 day and in 29% of eyes at 8 days after surgery using Visante anterior segment OCT. In their study, however, all eyes received stromal hydration and only 60% patients were examined at 8 days after surgery.[17]

In the cross-sectional image obtained with 3-D corneal and anterior segment OCT, the clear corneal incision showed an arcuate configuration, and its length was 1.86 ± 0.18 mm, with a range of 1.63 to 2.20 mm. Several studies have measured the dimension of clear corneal incisions using Visante anterior segment OCT.[8,16,23] Calladine and Packard reported mean clear corneal incision length of 1.61 ± 0.26 mm,[16] with a large range of values from 1.10 to 2.25 mm. Schallhorn and associates reported mean clear corneal incision length of 1.81 ± 0.27 mm, and their range was also large (1.41 to 2.39 mm).[24] Such discrepancy in the rage of clear corneal incision length measurements may be the result of the different surgical techniques and skills, but different measurement principles might have played a role. Visante anterior segment OCT captures only several cross-sectional images, and thus the longest direction of CCT may not be sectioned every time. However, 3-D corneal and anterior segment OCT creates 2-dimensional images by sectioning the 3-D image in any arbitrary directions, and therefore the longest part of the clear corneal incision perpendicular to the external or internal wound can be located easily.

Our study had several limitations. First, the study size was relatively small. Even with this sampling size, however, we could demonstrate clearly the influence of stromal hydration on corneal thickness and its time course. Second, we could not investigate the relationship between 5 architectural features and the stability of the clear corneal incision because all clear corneal incisions showed good water tightness in the current study. The stability of the clear corneal incision is thought to be important for the accession of bacteria to the intraocular space. Previous studies reported that the stability of the clear corneal incision was related with wound gaping and incision angle.[3,4,6] Further studies will be required to evaluate this relationship.

In conclusion, we have shown that the 3-D corneal and anterior segment OCT can evaluate the detailed architecture of a clear corneal incision noninvasively. The duration of stromal edema caused by intentional hydration also was evaluated. We demonstrated that stromal edema continued for at least 1 week, indicating that the sealing effect by stromal hydration lasts longer than clinically anticipated.

PUBLICATION OF THIS ARTICLE WAS SUPPORTED IN PART BY GRANTS-IN-AID 19390439 AND 19791256 FOR SCIENTIFIC RESEARCH from the Ministry of Education, Culture, Sports, Science and Technology, Tokyo, Japan. The authors indicate no financial conflict of interest. Involved in Design of study (S.F., K.K., T.O.); Conduct of study (S.F., K.K., Y.Y.); Collection (S.F., K.K.), management (S.F., K.K.), analysis (S.F., K.K., T.O.), and interpretation (S.F., K.K., T.O.) of data; and Preparation (S.F., T.O.), review (S.F., K.K., Y.Y., T.O.), and approval (S.F., K.K., Y.Y., T.O.) of the manuscript. The research protocol was approved by the Tsukuba University Hospital Institutional Review Board, and written informed consent was obtained from each patient. The study adhered to the tenets of Declaration of Helsinki.

## REFERENCES


1. Leaming DV. Practice styles and preferences of ASCRS members—2003 survey. J Cataract Refract Surg 2004;30(4): 892–900.
2. Vasavada AR, Praveen MR, Pandita D, et al. Effect of stromal hydration of clear corneal incisions: quantifying ingress of trypan blue into the anterior chamber after phacoemulsification. J Cataract Refract Surg 2007;33(10):623–627.
3. Taban M, Sarayba MA, Ignacio TS, Behrens A, McDonnell PJ. Ingress of India ink into the anterior chamber through sutureless clear corneal cataract wounds. Arch Ophthalmol 2005;123(5):643–648.
4. Herretes S, Stark WJ, Pirouzmanesh A, Reyes JM, McDonnell PJ, Behrens A. Inflow of ocular surface fluid into the anterior chamber after phacoemulsification through sutureless corneal cataract wounds. Am J Ophthalmol 2005; 140(4):737–740.
5. McDonnell PJ, Taban M, Sarayba M, et al. Dynamic morphology of clear corneal cataract incisions. Ophthalmology 2003;110(12):2342–2348.
6. Taban M, Rao B, Reznik J, Zhang J, Chen Z, McDonnell PJ. Dynamic morphology of sutureless cataract wounds—effect of incision angle and location. Surv Ophthalmol 2004; 49(Suppl 2):S62–S72.
7. Torres LF, Saez-Espinola F, Colina JM, et al. In vivo architectural analysis of 3.2 mm clear corneal incisions for phacoemulsification using optical coherence tomography. J Cataract Refract Surg 2006;32(11):1820–1826.
8. Fine IH, Hoffman RS, Packer M. Profile of clear corneal cataract incisions demonstrated by ocular coherence tomography. J Cataract Refract Surg 2007;33(1):94–97.
9. Yasuno Y, Madjarova VD, Makita S, et al. Three-dimensional and high-speed swept-source optical coherence tomography for in vivo investigation of human anterior eye segments. Opt Express 2005;13(26):10652–10664.
10. Yun S, Tearney G, de Boer J, Iftimia N, Bouma B. High-speed optical frequency-domain imaging. Opt Express 2003; 11(22):2953–2963.
11. Yun SH, Tearney G, de Boer J, Bouma B. Motion artifacts in optical coherence tomography with frequency-domain ranging. Opt Express 2004;12(13):2977–2998.
12. Kerbage C, Lim H, Sun W, Mujat M, de Boer JF. Large depth-high resolution full 3D imaging of the anterior segments of the eye using high speed optical frequency domain imaging. Opt Express 2007;15(12):7117–7125.
13. Miura M, Kawana K, Iwasaki T, et al. Three-dimensional anterior segment optical coherence tomography of filtering blebs after trabeculectomy. J Glaucoma 2008;17(3):193–196.
14. Kawana K, Yasuno Y, Yatagai T, Oshika T. High-speed, swept-source optical coherence tomography: a 3-dimensional view of anterior chamber angle recession. Acta Ophthalmol Scand 2007;85(6):684–685.
15. Miura M, Mori H, Watanabe Y, et al. Three-dimensional optical coherence tomography of granular corneal dystrophy. Cornea 2007;26(3):373–374.
16. Calladine D, Packard R. Clear corneal incision architecture in the immediate postoperative period evaluated using optical coherence tomography. J Cataract Refract Surg 2007; 33(8):1429–1435.
17. Dupont-Monod S, Labbé A, Fayol N, Chassignol A, Bourges JL, Baudouin C. In vivo architecture analysis of clear corneal incision using anterior segment optical coherence tomography. J Cataract Refract Surg 2009;35(3):444–450.
18. Marcon AS, Rapuano CJ, Jones MR, Laibson PR, Cohen EJ. Descemet's membrane detachment after cataract surgery: management and outcome. Ophthalmology 2002; 109(2):2325–2330.
19. Dowlut SM, Brunet M. Detachment of Descemet's membrane in cataract surgery. Can J Ophthalmol 1980;15(3): 122–124.
20. Aust W, Wernhard U. Defects of Descemet's membrane as a complication in cataract extraction with lens implantation. Dev Ophthalmol 1987;13:20–29.
21. Emery JM, Wilhelmus KA, Rosenberg S. Complications of phacoemulsification. Ophthalmology 1978;85(2):141–150.
22. Anderson CJ. Gonioscopy in no-stitch cataract incisions. J Cataract Refract Surg 1993;19(5):620–621.
23. Mackool RJ, Holtz SJ. Descemet membrane detachment. Arch Ophthalmol 1977;95(3):459–463.
24. Schallhorn JM, Tang M, Li Y, Song JC, Huang D. Optical coherence tomography of clear corneal incisions for cataract surgery. J Cataract Refract Surg 2008;34(9):1561–1565.

## Biosketch

Shinichi Fukuda graduated from Tsukuba University School of Medicine, Ibaraki, Japan in 2005. He is currently residency and fellowship at University of Tsukuba Hospital, Department of Ophthalmology.

# Quantitative Evaluation of Changes in Eyeball Shape in Emmetropization and Myopic Changes Based on Elliptic Fourier Descriptors

*Kotaro Ishii,*[1] *Hiroyoshi Iwata,*[2] *and Tetsuro Oshika*[1]

**Purpose.** To evaluate changes in eyeball shape in emmetropization and myopic changes using magnetic resonance imaging (MRI) and elliptic Fourier descriptors (EFDs).

**Methods.** The subjects were 105 patients (age range, 1 month–19 years) who underwent head MRI. The refractive error was determined in 30 patients, and eyeball shape was expressed numerically by principal components analysis of standardized EFDs.

**Results.** In the first principal component (PC1; the oblate-to-prolate change), the proportion of variance/total variance in the development of the eyeball shape was 76%. In all subjects, PC1 showed a significant correlation with age (Pearson $r = -0.314$; $P = 0.001$), axial length (AL, $r = -0.378$; $P < 0.001$), width ($r = -0.200$, $P = 0.0401$), oblateness ($r = 0.657$, $P < 0.001$), and spherical equivalent refraction (SER, $r = 0.438$; $P = 0.0146$; $n = 30$). In the group containing patients aged 1 month to 6 years ($n = 49$), PC1 showed a significant correlation with age ($r = -0.366$; $P = 0.0093$). In the group containing patients aged 7 to 19 years ($n = 56$), PC1 showed a significant correlation with SER ($r = 0.640$; $P = 0.0063$).

**Conclusions.** The main deformation pattern in the development of the eyeball shape from oblate to prolate was clarified by quantitative analysis based on EFDs. The results showed clear differences between age groups with regard to changes in the shape of the eyeball, the correlation between these changes, and refractive status changes. (*Invest Ophthalmol Vis Sci.* 2011;52:8585–8591) DOI:10.1167/iovs.11-7221

Peripheral visual input plays an important role in emmetropization, and the quality of the peripheral visual input may affect postnatal refractive eye development in patients with myopia. However, changes in the shape of the eyeball during normal and pathologic postnatal eye development are still poorly understood.[1–3] A previous report described that when the angle on the retinal side of the extrafoveal area changes by 1°, the contrast of the retinal image changes.[4] Therefore, a quantitative evaluation of the shape of the eyeball is necessary to understand eye growth during infancy.

Until now, few studies have been conducted on the shape of the eyeball itself.[1,5–7] Deller et al.[5] reported that the dimensions of most emmetropic eyes are similar, but that the rate of increase of length is approximately twice that of height and width as myopia increases. Atchison et al.[6] suggested that there are considerable individual variations in adult eyes. In general, myopic eyes are elongated relative to emmetropic eyes, with greater growth in length than height and even lesser growth in width. Moreover, some researchers determined that the variations are quantitative by using the Q-value of the shape of the surface of the adult retina.[8] Their study results showed that in both emmetropia and myopia, the retinal shape is oblate and that this oblateness is decreased according to the strength of the myopia.

The current method of evaluating the shape of the eyeball uses the ratio of the length, radius of curvature, angle of the tangent on the retinal surface, and Q-value.[1,4–8] However, limitations in the evaluation of partial features and problems with the inaccuracy and lack of reproducibility are persistent with the use of these evaluation methods. In addition, the Q-value is not suitable for the evaluation of complex shapes, such as the shape of the entire eyeball. Therefore, it is necessary to introduce a method that can mathematically achieve a quantitative evaluation of an outline of the shape of the eyeball.

Elliptic Fourier descriptors (EFDs), initially proposed by Kuhl and Giardina[9] in 1982, can numerically express any shape with a closed two-dimensional contour. There have been reports showing that measurements based on EFDs are helpful in the quantitation of plant and animal organ shapes.[10–17] Despite its potential, however, there have been relatively few reports on the use of EFDs in shape analysis within the field of clinical medicine. In our study, we used eyeball images taken by magnetic resonance imaging (MRI) to conduct a quantitative analysis of eyeball shape development based on EFDs.

## Materials and Methods

Informed consent was obtained from all patients participating in the present study or their guardians. The approval of the hospital's ethics committee was also obtained. The study was conducted in accordance with the guidelines of the Declaration of Helsinki. The study sample refers to 266 cases (ranging in age from 1 month to 19 years) in which magnetic resonance images (MRIs) of the head were obtained at regular physical checkups during a 6-month period from April to October 2008 at Tsukuba University Hospital. The exclusion criteria for analysis were intracranial space-occupying lesions, cerebral hemorrhage, cerebral contusions, hydrocephalus, congenital abnormalities, chromosomal abnormalities, metabolic diseases, and degenerative diseases, and the criteria were specified as the cases of those patients for whom the MRI results constituted "no abnormality." As a result, 105 cases were included in the analysis, 30 of which were evaluated for refractive error. The refractive error was measured with an autorefractometer in subjects under cycloplegia with atropine sulfate or cyclopentolate hydrochloride. In subjects younger than 6 years, 0.5% atropine sulfate was applied with eyedrops. In addition, the MRIs and

From the [1]Department of Ophthalmology, Institute of Clinical Medicine, University of Tsukuba, Ibaraki, Japan; and the [2]Laboratory of Biometry and Bioinformatics, Department of Agricultural and Environmental Biology, Graduate School of Agricultural and Life Sciences, The University of Tokyo, Tokyo, Japan.

Submitted for publication January 13, 2011; revised March 3, April 4, July 21, August 12, and September 10, 2011; accepted September 28, 2011.

Disclosure: **K. Ishii**, None; **H. Iwata**, None; **T. Oshika**, None

Corresponding author: Kotaro Ishii, Department of Ophthalmology, Institute of Clinical Medicine, University Hospital of Tsukuba, 2-1-1 Amakubo, Tsukuba, Ibaraki 305-8576, Japan; ishii_k@md.tsukuba.ac.jp.

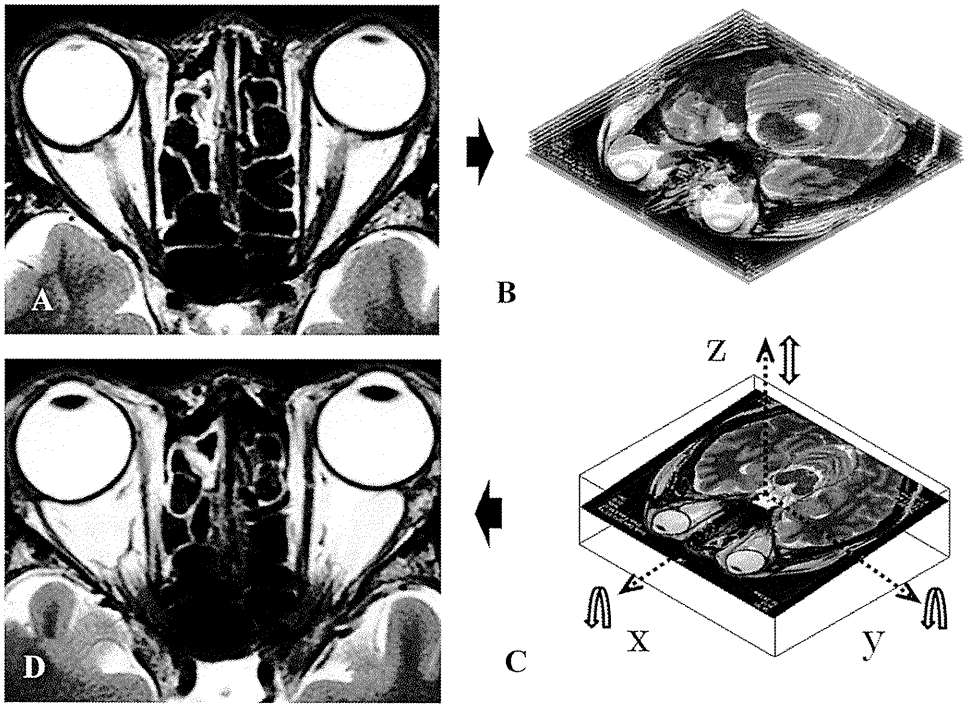


**FIGURE 1.** (**A**) In the unprocessed MRI, it was confirmed that the bilateral lenses, optic nerves, medial and lateral rectus muscles, and optic chiasm were depicted clearly in the horizontal images. (**B**) A 3D restructuring of the head MRIs from the horizontal MRI of a 3-mm slice. (**C**) To adjust the working reference plane, the optic chiasm of the unprocessed MRI was set to the intersection graph. The *y*-axis was set in parallel with both eyeballs. In addition, the *x*-axis was set orthogonal to the *y*-axis. The *z*-axis was vertically set as the working reference plane, orthogonal to the *x*- and *y*-axes. The *x*-axis was rotated to create a shape that ensured that the crystalline lenses of both eyes appeared the same. Then the *y*-axis was rotated so that the anterior chamber is at its greatest depth. Finally, the z-axis was moved up and down so that the crystalline lens might attain its maximum size; (**D**) A restructured horizontal MRI of patient 4 (Table 1, 73 years, female).

refractive error of seven subjects without ocular or intracranial diseases were measured for MRI validation.

MRIs were obtained with a 1.5-Tesla superconducting magnet (Gyroscan Intera and Gyroscan Power Trak 1000; Philips Medical Systems, Best, The Netherlands) with a phased-array head coil. Horizontal $T_1$- and $T_2$-weighted images were obtained for all patients. $T_2$-weighted images were obtained using the fast spin-echo method, with a pixel bandwidth of 100 to 150 kH, repetition time (TR) of 2500 to 2948 ms, echo time (TE) of 90 to 130 ms, section thickness of 1.2 to 3 mm, field of view of 70 × 70- to 95 × 95-mm, image frequency of 63.9, pixel spacing of 0.429 to 0.625 pixel/mm, flip angle of 90°, and an acquisition matrix of 256 × 256 to 320 × 320. $T_1$-weighted images were obtained with a spin-echo sequence with a TR of 480 to 574 ms, TE of 14 to 18 ms, section thickness of 1.2 to 3 mm, image frequency of 63.9, pixel spacing of 0.313 to 0.429 pixel/mm, and flip angle of 90°.

All patients were imaged while supine, and those aged 6 years or younger were sedated. All ocular dimension measurements were made from the horizontal images at approximately 16 magnifications on a computer monitor with a standard resolution of 512 × 512 pixels. The distances were measured with a line caliper in a software program, and the distance between the two points was converted from pixels to millimeters by using pixel-spacing data. Axial length (AL) and width of the right eye were measured from the horizontal MRIs. As the $T_2$-weighted images were used to apply EFDs, the shaft length of the inside of the eyeball was measured in the AL measurements. AL was recorded as the distance between the posterior cornea and the approximate location of the fovea along the line that bisected the eye in the horizontal plane. The eye width was measured between the retinal surfaces on either side across the horizontal image at the point that visually appeared the widest.

## MRI Validation

As our examinations were part of a retrospective study and the MRIs of the infants in that study were taken with the subjects under sedation, it was not possible to fix the visual line on these images. Therefore, a

**TABLE 1.** A Comparison of Axial Lengths Determined by MRI and A-scan Ultrasonography

| Participant Age, Sex | Eye | Mean SER (D) | A-scan US AL (mm) | MRI-AL (mm) | 3D-AL (mm) | (A-scan US AL) Minus (MRI-AL) | (A-scan US AL) Minus (3D-AL) |
|---|---|---|---|---|---|---|---|
| 56, female | Right | −0.75 | 23.53 | 23.31 | 23.5 | 0.22 | 0.03 |
| | Left | −0.5 | 23.39 | 23.08 | 23.5 | 0.31 | −0.11 |
| 73, male | Right | −1.25 | 25.31 | 24.41 | 24.8 | 0.9 | 0.51 |
| | Left | −0.75 | 25.21 | 24.8 | 25 | 0.41 | 0.21 |
| 63, female | Right | 0.5 | 22.9 | 22.86 | 22.9 | 0.04 | 0 |
| | Left | 0.75 | 22.83 | 22.64 | 23.1 | 0.19 | −0.27 |
| 73, female | Right | −2.5 | 23.84 | 23.2 | 23.7 | 0.64 | 0.14 |
| | Left | −1.75 | 23.57 | 22.9 | 23.6 | 0.67 | −0.03 |
| 72, male | Right | −1.5 | 23.39 | 23.18 | 23.3 | 0.21 | 0.09 |
| | Left | −1.75 | 23.57 | 23.43 | 23.1 | 0.14 | 0.47 |
| 30, male | Right | −2.25 | 25.31 | 25.48 | 25.1 | −0.17 | 0.21 |
| | Left | −2.00 | 25.21 | 24.96 | 25.6 | 0.25 | −0.39 |
| 62, female | Right | 0.75 | 22.95 | 22.87 | 22.9 | 0.08 | 0.05 |
| | Left | 0.25 | 23.12 | 22.65 | 22.9 | 0.47 | 0.22 |
| Mean ± SD | | | 23.87 ± 0.96 | 23.56 ± 0.94 | 23.79 ± 0.93 | 0.31 ± 0.28 | 0.08 ± 0.25 |

A-scan US, A-scan ultrasonography; 3D, the three-dimensional restructured image.

technique using three-dimensional (3D) MRIs of the eyeball was used to obtain the horizontal MRIs of the eyeball in all analyses at an equal height. We used the unprocessed horizontal MRIs from approximately 7 to 15 unprocessed slices to make the 3D MRI of the eyeball (Figs. 1A, 1B). The *x*-, *y*-, and *z*-axes of these 3D images have been adjusted respectively (ZedView software program; Lexi Corp., Tokyo, Japan), as shown in Figure 1.

The initial experiments confirmed that the bilateral lenses, optic nerves, medial and lateral rectus muscles, and optic chiasm were depicted clearly in the unprocessed horizontal MRIs. In addition, a slice was made in the working reference plane of the rotation. The center of the rotation axis used the optic chiasm to facilitate identification of the position of the eyeball and grasp of the rotation state. The *y*-axis was set parallel to both eyeballs, as shown in Figure 1C. In addition, the *x*-axis was set orthogonal to the *y*-axis. The *z*-axis was vertically set as the working reference plane, orthogonal to the *x*- and *y*-axes. To create a shape that ensured that the crystalline lenses of both eyes appeared the same, the *x*-axis was rotated. Then the *y*-axis was rotated so that the anterior chamber is at its greatest depth. Finally, the *z*-axis was moved up and down so that the crystalline lens could attain its maximum size. In this study, the MRIs from the 1.2- to 3-mm slices were used.

In the evaluation and examination, the measurement of AL by A-scan ultrasonography (AL-3000; TOMEY, Nagoya, Japan) was compared in seven subjects (14 eyes) with that based on the MRI. The MRI of the 3-mm slice was used for evaluation and examination to ensure an error margin for the region. Because the AL based on the MRI did not contain the corneal thickness, AL based on A-scan ultrasonography was a value from which the corneal thickness had been subtracted. The results of the MRI validation are shown in Table 1. AL determined by A-scan ultrasonography showed a significant correlation with that generated by the unprocessed MR (Pearson $r = 0.956$; $P < 0.001$) and 3D restructured ($r = 0.966$; $P < 0.001$) images. A Bland-Altman plot, indicating the relationship between AL generated by the unprocessed MR and 3D restructured images with that based on A-scan ultrasonography was made, as shown in Figure 2. Because the horizontal image of the unprocessed MRI did not usually cut an eyeball at a major axis, AL determined from the unprocessed MRI was shorter than the actual length (Table 1). In addition, there was a significant difference between the error margin of AL determined by a combination of A-scan ultrasonography and the 3D-restructured image and the error margin of AL determined by a combination of A-scan ultrasonography and the unprocessed MRI (paired *t*-test, $P = 0.0191$). In this study, therefore, we used the $T_2$-weighted horizontal MRIs that used the 3D restructuring technique to estimate the geometry of the eyeball.

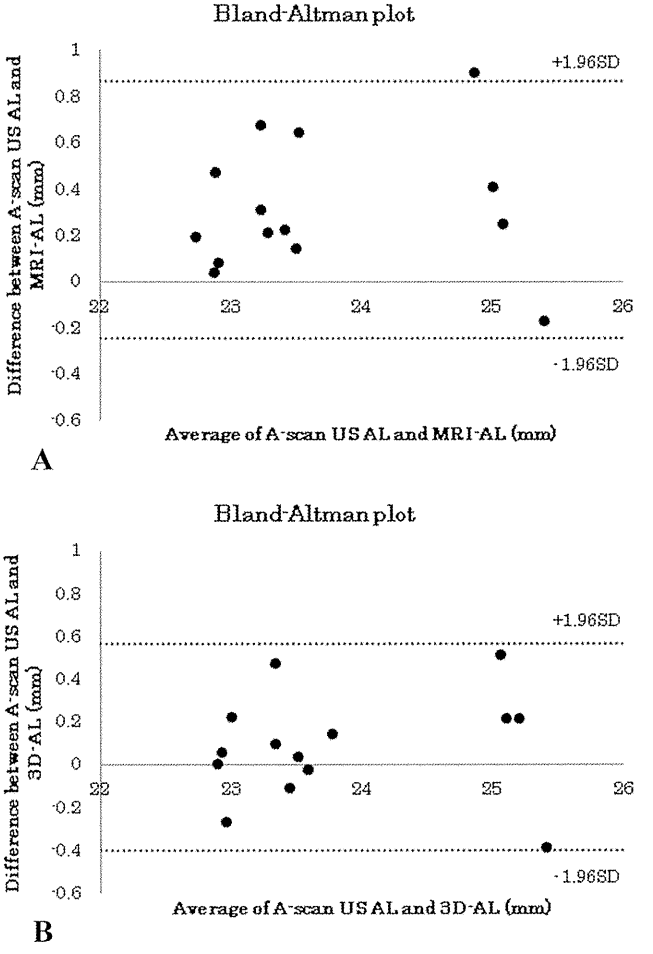


**FIGURE 2.** Bland-Altman plots indicating the relationship between AL generated by the unprocessed MR and 3D restructured images and that based on A-scan ultrasonography. A-scan US, A-scan ultrasonography. (**A**) The mean value of the difference between the A-scan-US AL and MRI AL was 0.31. The average difference ±1.96 SD was from −0.24 to 0.87. (**B**) The mean value of the difference between the A-scan-US AL and 3D AL was 0.081. The average difference ±1.96 SD was from −0.40 to 0.57.

## Elliptic Fourier Descriptors

To obtain a sharply defined contour of the eyeball, the $T_2$-weighted MRIs were used for elliptic Fourier descriptors (EFDs; Fig. 3A). In all cases, images of the right eyes were used for image processing and contour recording. In the derivation of EFDs, the *x*- and *y*-coordinate information of the contour of eyeball was taken in the form of a closed curve, as is illustrated in Figure 3B. The shape was mathematically delineated with the Fourier series expansion of the closed curve. The obtained Fourier coefficients ($a_n$, $b_n$, $c_n$, and $d_n$) were further standardized to be invariant under a change of size and direction of a contour and starting point of contour trace. In this study, standardization was done on the basis of the two landmark points that were used in axial length measurements. In standardizing EFDs, the corneal apex of the right eye was placed on the right, the temporal side on the top, and the nasal side at the bottom (Fig. 3C).

With regard to the harmonic number $n$, the larger the maximum value of $n$ becomes, the better the descriptive power of the shape. In this analysis, the value of $n$ was set at 20 ($n = 20$). When $n = 20$, the standardized EFDs comprise 80 standardized Fourier coefficients. Since the number of coefficients was large, it was not easy to analyze the variation of each coefficient and understand the results of the analysis. To summarize the information contained in the EFDs, we conducted a principal component analysis (PCA) of EFDs. The PCA reduced the dimension of the original data (i.e., 80) to a much lower dimension. The PCA was performed based on the variance-covariance matrix of the coefficients, and the component scores of the first several components were used as the measurements of the eyeball shape (Fig. 3D). The shape analysis method that uses standardized EFDs evaluates the shape provided from an eyeball image (such as Fig. 3A) by several shape principal components ($s_1$, $s_2$, $s_3$, ...), as shown in Figure 3D.

## Evaluation of Oblateness

Oblateness indicates the shape of a spheroid body compared with that of a sphere. Oblateness $f$ is defined as $f = 1 - AL/a$, where $a$ is the equatorial diameter. For an oblate spheroid for which $a > AL$, $f > 0$, and for a prolate spheroid for which $a < AL$, $f < 0$. For a sphere, $f = 0$.

## Statistical Analyses

The measurements of the eye dimensions of AL and width were recorded in millimeters and are expressed as the mean ± standard deviation. The Pearson correlation coefficients, determined using a bivariate correlation analysis, were used to compare factors such as AL,

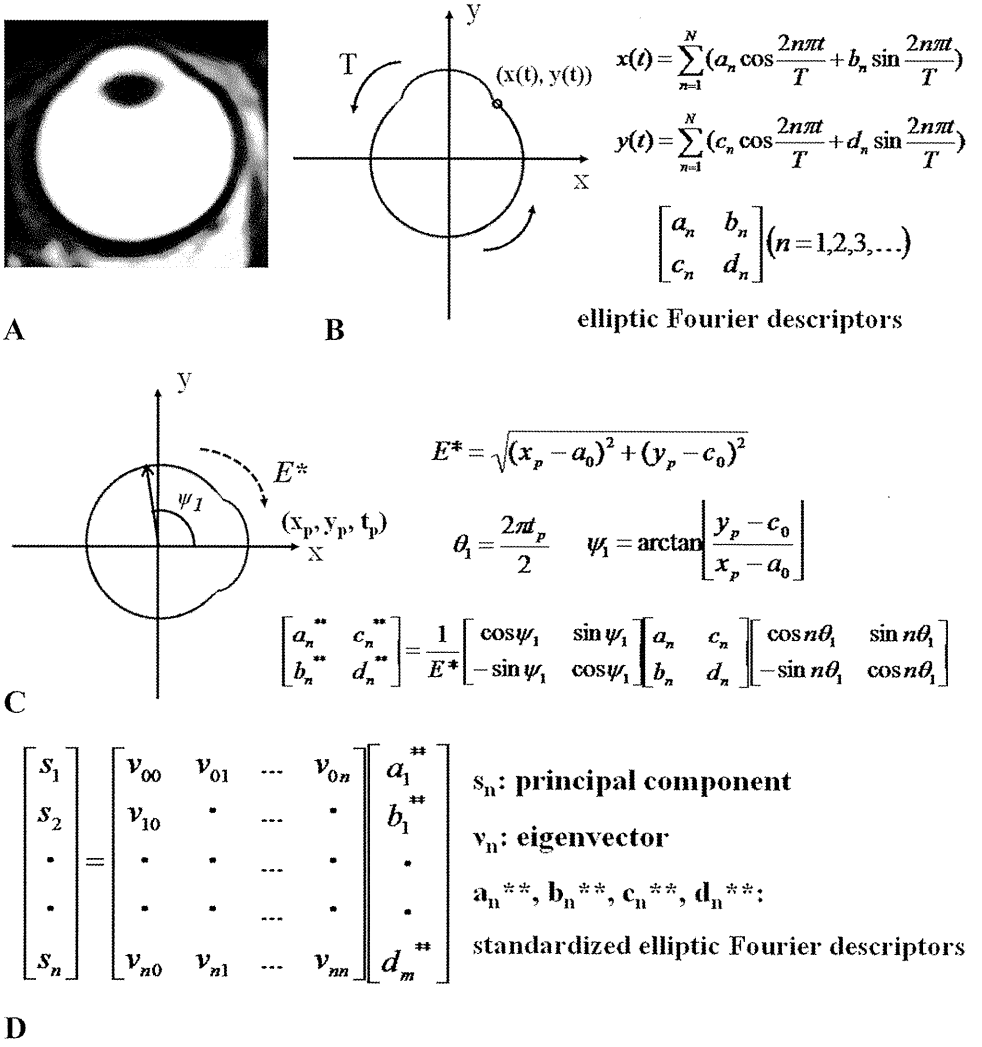


FIGURE 3. (A) In reference to the $T_2$-weighted MRIs that were obtained of the right eye. (B) The closed curve on the graph refers to the seam of the contour that was image processed from the eyeball images derived via MRI. The $x$ and $y$ coordinates of the contour are delineated, respectively, as periodic functions of distance $t$ with a period of $T$. (C) The location of point $E^*$ on the graph, which is a reference point for standardizing the elliptic Fourier descriptors obtained in (B) was identified manually. With this standardization, the size and direction of all contours were aligned, respectively, to the size and direction of the corneal apex on the right eyeball. (D) A PCA was performed based on the variance-covariance matrix of the coefficients.

width, age, principal components of standardized EFDs, and oblateness. $P \leq 0.05$ was significant (StatView ver. 5.0; SAS, Cary, NC).

## RESULTS

There were 105 patients (105 eyes) enrolled in the study; they consisted of 55 males and 50 females, ranging in age from 1 month to 19 years (8.47 ± 6.64 years). The AL (Pearson $r$ = 0.794; $P < 0.001$) and width ($r$ = 0.754; $P < 0.001$) of the right eyes showed a significant correlation with age. AL and age were closely approximated via a logarithmic approximation. AL (Pearson $r$ = −0.443; $P < 0.001$) and age ($r$ = −0.356; $P$ = 0.002) showed a significant correlation with oblateness (Figs. 4A, 4B). The average of the spherical equivalent refraction (SER) was −0.68 ± 1.19 D ($n$ = 30). The SER showed a significant correlation with AL ($r$ = −0.695, $P < 0.001$), width ($r$ = −0.547; $P$ = 0.0014), oblateness ($r$ = 0.423; $P$ = 0.0189), and age ($r$ = −0.682; $P < 0.001$).

A PCA was performed based on the variance-covariance matrix of the coefficients (Fig. 3D). Therefore, each principal component was independent of the shape without the correlation. In the PCA of standardized EFDs, the proportion of the variance/total variance of the first principal component (PC1) was 76.0%. The proportions of PC2 and PC3 were 7.7% and 4.1%, respectively. Figure 5 shows the changes in shape variations within the value range of −2 to 2 SD for the three principal components. The solid line in Figure 5 indicates the average value, and the numerical value is set at 0 in the PCA. The dotted line represents −2 SD, and the dashed line represents 2 SD. Regarding the components following PC4, their ratio to the eyeball shape was small, and the change was minute. As a result, it was found that PC1 showed a significant correlation with age (Pearson $r$ = −0.314; $P$ = 0.001) as well as with AL ($r$ = −0.378; $P < 0.001$), width ($r$ = −0.200; $P$ = 0.0401), and oblateness ($r$ = 0.657; $P < 0.001$; Fig. 4C). PC1 also was significantly correlated with SER ($r$ = 0.438, $P$ = 0.0146; $n$ = 30). PC2 showed a significant correlation with oblateness (Pearson $r$ = −0.289, $P$ = 0.0027), but not AL (Fig. 4D). PC1 and -2 almost intersected oblateness in the origin (Figs. 4C, 4D). Therefore, the eyeball shape of the mean value of PC1 and -2 was approximately spherical.

Emmetropization is usually completed by about age 6 years. For those subjects in the group aged 1 month to 6 years ($n$ = 49), AL (Pearson $r$ = 0.733; $P < 0.001$), width ($r$ = 0.681; $P < 0.001$), and oblateness ($r$ = −0.309; $P$ = 0.0301) showed a significant correlation with age. PC1 showed a significant correlation with AL ($r$ = −0.421; $P$ = 0.0024), oblateness ($r$ = −0.715; $P < 0.001$), and age ($r$ = −0.366; $P$ = 0.0093), whereas PC2 only showed a significant correlation with oblateness ($r$ = −0.355; $P$ = 0.0118). The average SER of the younger subjects was 0.09 ± 0.75 D (age, 1 month–6 years; $n$ = 14). For those subjects aged 7 to 19 years ($n$ = 56), AL ($r$ = 0.459; $P$ = 0.003) and width ($r$ = 0.312; $P$ = 0.0187) showed a significant correlation with age. This result seems to reflect